JPET Fast Forward. Published on December 27, 2010 as DOI: 10.1124/jpet.110.176677

Pharmacokinetic-Pharmacodynamic Modeling of Rifampicin-Mediated *Cyp3a11* Induction in SXR Humanized Mice

Joseph J. Raybon, Devin Pray, Daniel G. Morgan, Mary Zoeckler, Ming Zheng, Michael Sinz and Sean Kim

Discovery Metabolism and Pharmacokinetics (J.J.R., M.Z., M.S., S.K.), Lead Profiling (D.P.) and Bioanalytical Research (D.G.M.), Bristol-Myers Squibb, Wallingford, Connecticut; and Discovery Medicine and Clinical Pharmacology (M.Z.), Bristol-Myers Squibb, Hopewell, New Jersey

JPET Fast Forward. Published on December 27, 2010 as DOI: 10.1124/jpet.110.176677
This article has not been copyedited and formatted. The final version may differ from this version.

Running Title: In Vivo Modeling of Rifampicin-Mediated Induction

Corresponding author: Dr. Joseph J. Raybon, Metabolism and Pharmacokinetics, Bristol-Myers Squibb, 5 Research Parkway, Wallingford, CT 06492

Email: joseph.raybon@bms.com

Telephone: (203) 677-5033

Fax: (203) 677-6193

The number of text pages: 21

The number of tables: 4

The number of figures: 6

The number of references: 21

The number of words in abstract: 250

The number of words in introduction: 648

The number of words in discussion: 1508

Abbreviations

AUC; area under the curve, C_{max}; maximum concentration, DDI; drug-drug interaction, PK-PD; pharmacokinetic-pharmacodynamic, PXR; pregnane-X-receptor, SXR; steroid and xenobiotic-X-receptor, CAR; constitutive androstane receptor, RIF; rifampicin, CYP; cytochrome P450, SC50; concentration at 50% maximum stimulus, Smax; maximum stimulus the drug can produce, PBPK; physiologically-based pharmacokinetic model, P.O.; by mouth, Q.D.; once daily, RNA; ribonucleic acid, mRNA; messenger ribonucleic acid, TRZ; triazolam, DMSO; dimethyl sulfoxide, RT-PCR; reverse-transcriptase polymerase chain reaction, PEG400; polyethyleneglycol 400, LC/MS-MS; liquid chromatography with tandem mass spectrometry

Recommended Section Assignment

Metabolism, Transport and Pharmacogenomics

Abstract

The purpose of this study was to develop a mechanistic pharmacokinetic-pharmacodynamic (PK-PD) model to describe the effects of rifampicin on hepatic *Cyp3a11* RNA, enzymatic activity and triazolam pharmacokinetics. Rifampicin was administered to SXR humanized mice at 10 mg/kg (P.O.; Q.D. for 3 days) followed by triazolam (4 mg/kg, P.O.) 24 h after the last dose of rifampicin. Rifampicin and triazolam concentrations, *Cyp3a11* RNA expression and activity in the liver were measured over the 4-day period. Elevations in *Cyp3a11* RNA expression were observed 24 h after the first dose of rifampicin, reaching a maximum (~10-times baseline) after the third dose and were sustained until day 4 and began declining 48 h after the last rifampicin dose. Similar changes in enzymatic activity were also observed. The triazolam serum AUC was 5-fold lower in mice pretreated with rifampicin, consistent with enzyme induction. The final PK-PD model incorporated rifampicin liver concentration as the driving force for the time-delayed *Cyp3a11* induction governed by *in vitro* potency estimates; which in turn regulated the turnover of enzyme activity. The PK-PD model was able to recapitulate the delayed induction of *Cyp3a11* mRNA and enzymatic activity by rifampicin. Furthermore, the model was able to accurately anticipate the reduction in the triazolam plasma AUC by integrating a ratio of the predicted induced enzyme activity and basal activity into the equations describing the triazolam pharmacokinetics. In conjunction with the SXR humanized mouse model, this mathematical approach may serve as a tool for predicting clinically relevant drug-drug interactions via PXR-mediated enzyme induction and possibly extended to other induction pathways (e.g. CAR).

Introduction

The induction of drug metabolizing enzymes often leads to a reduced level of therapeutically active parent drug or increased production of reactive metabolites. The clinical manifestation of such events range from loss of therapeutic efficacy to increased toxicity of drugs that are metabolized by these enzyme(s) (Lin, 2006). As such, screening for potential inducers has been at the core of lead optimization during drug development (Tucker et al., 2001; Hewitt et al., 2007a). In order to aid in screening, many *in vitro* tools have been developed, which can be grouped into two approaches; utilization of the receptor-ligand interaction and the employment of hepatocyte or hepatocyte-like cells. Pregnane-X-Receptor (PXR) ligand binding and transactivation assays have been widely used to rapidly screen potential inducers of CYP3A4, CYP2B6, CYP2C and transporters (e.g., MRP-2 and PGP) (Zhu et al., 2004; Sinz et al., 2006), while the primary human hepatocyte model is recognized as a gold standard assay throughout the pharmaceutical industry and regulatory agencies as it readily responds to a wide variety of inductive stimuli, even beyond those mediated by PXR (Hewitt et al., 2007b). There are also several known immortalized cell lines (such as Fa2N-4 and HepaRG), which mimic primary hepatocytes in their induction responses (Ripp et al., 2006; Hariparsad et al., 2008; McGinnity et al., 2009).

At issue with these current practices is the tendency to focus on providing a qualitative measure of the magnitude of induction. In addition, the potency of the inducer is studied under static conditions and ignores the relationship between exposure of the inducer and time, the resultant alterations in mRNA levels and enzymatic activity, and the downstream impact on the pharmacokinetics of a specific probe substrate. In order to

study this dynamic/temporal relationship between inducers and the downstream induction response, one has to investigate such events *in vivo*. Animal models that can provide a quantitative measure of the magnitude of a drug-drug interaction (DDI) are, however, limited due to species differences in induction responses. Humanization of mice by replacing mouse PXR with the human homologue (SXR, steroid and xenobiotics X receptor) overcomes this obstacle and opens the possibility of using mice as a quantitative model to predict human CYP3A4 induction (Xie et al., 2000). Availability of such models is particularly valuable during the early stages of compound selection and lead optimization, as chemical modifications could still be performed to mitigate the potential for serious induction liabilities.

Previously, we described the use of an SXR humanized mouse model that accurately quantified the impact of rifampicin-mediated *Cyp3a11* induction on RNA expression, enzyme activity and triazolam pharmacokinetics *in vivo* (Kim et al., 2008). While the study demonstrated a good correlation of triazolam AUC reduction between SXR humanized mice and humans under similar *in vivo* exposures, it required resource-intensive repeat-dose studies to identify the rifampicin dose that produced therapeutically relevant exposures and a corresponding *Cyp3a11* RNA induction response.

The objective of the current investigation was to find a more efficient way to conduct DDI studies in SXR humanized mice without significantly comprising predictability. To this end, we attempted to create a mathematical framework that would eventually provide a prediction of the magnitude of change in the pharmacokinetics of a probe substrate in SXR humanized mice (and ultimately in patients) utilizing only knowledge of the *in vitro* potency in mouse hepatocytes and single-dose *in vivo*

pharmacokinetics of the inducer. Using rifampicin as a prototypical inducer, we characterized the time course of Cyp3a11 RNA induction and down-stream elevations in CYP3A11 enzyme activity using a turnover model, wherein the *in vitro* induction potency ($S_{max,RIF}$ and $SC_{50,RIF}$) of rifampicin was fixed as a constant and the impact on the pharmacokinetics of a CYP3A11 probe-substrate was simulated. This approach allowed for estimation of the rates governing the system-dependent synthesis and degradation of this pathway which could be used for future predictions/simulations of the induction potential of unknown compounds given a measure of the compound-dependent *in vitro* potency.

Materials and Methods

Chemicals and Reagents. Rifampicin, triazolam, and PEG400 (polyethylene glycol-400) were obtained from Sigma Chemical Co. (St. Louis, MO). 1-Hydroxytriazolam was purchased from Biomol (Plymouth Meeting, PA). Turbocatcher 96 mRNA and RNeasy 96 total RNA isolation kits were purchased from Qiagen (Valencia, CA). Taqman® primers and sequence detection probes were obtained from Applied Biosystems (Foster City, CA). The generic names for all commonly used chemical reagents have been used.

Experimental Animals. SXR humanized mice were bred at Bristol-Myers Squibb (Wallingford, CT). Mice were provided food and water *ad libitum* and housed in a temperature-controlled room under a 12 h light/dark cycle. All studies were conducted in accordance with the Principles of Laboratory Animal Care (NIH Publication No. 85-23, revised in 1985).

SXR Humanized Mouse Hepatocyte Induction Study. Mouse hepatocytes were freshly isolated from SXR humanized mice and plated onto 24-well collagen-coated plates at CellzDirect (Durham, NC). Following a 24 h acclimation, hepatocytes were incubated in a serum-free William's E media containing either DMSO (0.1% v/v) or rifampicin (0.4 to 50 μM in 0.1% DMSO) for 3 consecutive days. The hepatocytes were then incubated with lysis buffer from a SV-96^{TM} RNA purification kit (Promega, Madison, WI). The purified RNA was then used in a real-time RTPCR to measure the expression of *Cyp3a11* RNA as described previously (Kim et al., 2008). Non-linear regression analysis for determination of the capacity ($S_{max,RIF}$) and sensitivity ($SC_{50,RIF}$) parameters was performed with GraphPad Prism v4.0 for Windows (GraphPad Software, San Diego, CA).

In Vivo Induction Studies in SXR Humanized Mice. Male SXR humanized mice were dosed orally with 10 mg/kg rifampicin or vehicle (80/20 PEG400/water) once daily for 3 days. On day 4, all animals were dosed orally with 4 mg/kg triazolam (50/50 PEG400/saline). Following each daily dose of rifampicin (days 1-3), mice were euthanized at 0.5, 1, 2, 4, 8 and 24 h post-dose (N=3 mice/time point). Blood was collected by cardiac puncture and centrifuged to obtain serum. Liver tissue was also harvested and a portion was preserved in RNALater and stored at 4°C for subsequent RNA isolation. Both serum samples and an additional piece of liver were frozen at -20°C for subsequent rifampicin and triazolam quantitation. The remaining liver tissues were frozen at -80°C for microsomal preparation. On day four, 24 h following the final dose of rifampicin, all rifampicin and vehicle treated mice were euthanized at various time points (0.08, 0.17, 0.33, 0.5, 0.75, 1, 2, 4, 6, 8 and 24 h) following triazolam administration (3 mice/time point). Similarly, a group of animals receiving vehicle on day 1 were euthanized and samples were collected as described above to establish basal *Cyp3a11* mRNA expression and CYP3A11 enzyme activity levels. Taqman™ RTPCR, microsomal isolation/incubation and LC/MS-MS analysis of rifampicin and triazolam were performed as described previously (Kim et al., 2008).

Pharmacokinetic/Pharmacodynamic Model. Using a naive-pooled approach, noncompartmental pharmacokinetic analysis was performed on the mean rifampicin plasma and liver concentration versus time profiles on days 1-3 and on the mean triazolam plasma concentration versus time profiles on the fourth day of the study using WinNonlin 5.0 (Mountain View, CA). A semi-physiological based PK-PD model describing the time course of rifampicin concentration in the blood and liver, its induction

of the *Cyp3a11* pathway and the downstream effects on the pharmacokinetics of triazolam is shown in Fig 1. Compartmental analysis was performed by first fitting the pharmacokinetic components of the model. The drug is introduced into the gut followed by first-order absorption into the liver where it is distributed to a secondary compartment which constitutes the plasma and the rest of the body. The hepatic elimination of rifampicin was described by a well-stirred model (Wilkinson, 1987). Equations 1 and 2 describe the gut and hepatic disposition of rifampicin following oral administration:

$$\frac{dA_{Gut,RIF}}{dt} = -k_{a,RIF} * A_{Gut,RIF} \quad (1)$$

$$V_H \frac{dC_{liver,RIF}}{dt} = k_{a,RIF} * A_{Gut,RIF} - \frac{Q_H}{V_H} * A_{liver,RIF} + k_{s,RIF} * A_{plasma,RIF} - \frac{CL_{H,RIF}}{V_H} * A_{liver,RIF} \quad (2)$$

where $k_{a,RIF}$, $A_{Gut,RIF}$, $A_{liver,\ RIF}$, $A_{plasma,\ RIF}$ and $C_{liver,\ RIF}$ represent the first-order absorption rate constant, the amount of rifampicin in the gut, liver and plasma compartment and the hepatic rifampicin concentration, respectively. The hepatic blood flow (Q_H) and liver volume (V_H) were fixed physiological parameters (Davies and Morris, 1993) and $k_{s,RIF}$ represents the first-order distribution rate from the plasma compartment to the liver. The hepatic extraction, clearance and bioavailability of rifampicin ($E_{H,RIF}$; $CL_{H,RIF}$; $F_{H,RIF}$) was described by a well-stirred model according to equations 3-5:

$$E_{H,RIF} = CL_{int,RIF} * f_{u,RIF} / (Q_H + CL_{int,t,RIF} * f_{u,RIF}) \quad (3)$$

$$CL_{H,RIF} = Q_H * E_{H,RIF} \quad (4)$$

$$F_{H,RIF} = 1 - E_{H,RIF} \quad (5)$$

where $E_{H,RIF}$ is the hepatic extraction, $CL_{int,RIF}$ is the intrinsic clearance and $f_{u,RIF}$ is the experimentally determined plasma unbound fraction (Bauer et al., 2006). The differential

JPET Fast Forward. Published on December 27, 2010 as DOI: 10.1124/jpet.110.176677
This article has not been copyedited and formatted. The final version may differ from this version.

equation governing the rate of change in the plasma compartment is described in equation 6:

$$V_{plasma,RIF}\frac{dC_{plasma,RIF}}{dt}=\frac{Q_H}{V_H}*F_{H,RIF}*A_{liver,RIF}-k_{s,RIF}*A_{plasma,RIF} \quad (6)$$

where $A_{plasma,RIF}$ and $C_{plasma,RIF}$ represent the amount and concentration of rifampicin in the plasma, respectively, and $V_{plasma,RIF}$ is the plasma volume of distribution. The first order distribution of rifampicin from the liver to the plasma is driven by hepatic plasma flow (Q_H) and the hepatic bioavailability ($F_{H,RIF}$).

The final parameters obtained from the pharmacokinetic fitting were then fixed and used to fit the pharmacodynamic data. The pharmacodynamic component of this model is also shown in Fig. 1. The differential equations used to describe the rate of change of *Cyp3a11* mRNA expression (*Cyp3a11*$_m$) are given in equations 7-10:

$$\frac{dTC_1}{dt}=\frac{1}{\tau}(Cyp3a11_m-TC_1) \quad (7)$$

$$\frac{dTC_2}{dt}=\frac{1}{\tau}(TC_1-TC_2) \quad (8)$$

$$\frac{dTC_3}{dt}=\frac{1}{\tau}(TC_2-TC_3) \quad (9)$$

$$Cyp3a11_m=\frac{S_{max,RIF}*C_{liver,RIF}}{SC_{50,RIF}+C_{liver,RIF}} \quad (10)$$

where the stimulatory effects of rifampicin on *Cyp3a11* mRNA levels (*Cyp3a11*$_m$) were described using a series of three transit compartments (TC_n) to account for the onset delay, with a transit time of Tau (τ). The hepatic rifampicin concentrations ($C_{liver,RIF}$) were responsible for stimulation of *Cyp3a11*$_m$ involving both capacity ($S_{max,RIF}$) and

JPET Fast Forward. Published on December 27, 2010 as DOI: 10.1124/jpet.110.176677
This article has not been copyedited and formatted. The final version may differ from this version.

sensitivity ($SC_{50,RIF}$) parameters which were fixed as constants based upon *in vitro* *Cyp3a11* RNA induction response in SXR mouse hepatocytes.

The expression of CYP3A11 enzyme activity and CYP3A11 protein levels were assumed to be proportional to one another and translated from $Cyp3a11_m$. The regulation of CYP3A11 enzyme activity was described by two first-order rate constants governing the $Cyp3a11_m$-dependent production ($k_{syn,CYP3A11}$) and loss of activity ($k_{deg,CYP3A11}$). The amplification factor (γ) indicates that multiple copies of protein are translated from a single copy of *Cyp3a11* mRNA. The equation describing the regulation of CYP3A11 activity is given in equation 11:

$$\frac{dCYP3A11}{dt} = k_{syn,CYP3A11} * TC_3^{\gamma} - k_{deg,CYP3A11} * CYP3A11 \quad (11)$$

The initial conditions for equations 7 and 11 were defined as $Cyp3a11_{m(0)}$ and $CYP3A11_{(0)}$ and were assumed to be stationary. The first-order degradation rate constant, $k_{deg,CYP3A11}$, can then be expressed as follows:

$$k_{deg,CYP3A11} = \frac{k_{syn,CYP3A11} * Cyp3a11_{m(0)}^{\gamma}}{CYP3A11_{(0)}} \quad (12)$$

For the CYP3A11 probe substrate, triazolam, disposition in the plasma was described using a one-compartment pharmacokinetic model with first-order oral absorption ($k_{a,TRZ}$) and linear elimination ($k_{el,TRZ}$) as described in equations 13 and 14:

$$\frac{dA_{TRZ}}{dt} = -k_{a,TRZ} * A_{TRZ} \quad (13)$$

$$V_{plasma,TRZ}/F_{TRZ} \frac{dC_{plasma,TRZ}}{dt} = k_{a,TRZ} * A_{TRZ} - k_{el,TRZ} * A_{plasma,TRZ} * M \quad (14)$$

Where, A_{TRZ} is the amount of triazolam in the absorption compartment and $A_{plasma,TRZ}$ and $C_{plasma,TRZ}$ is the amount and concentration of triazolam in the plasma. The term

JPET Fast Forward. Published on December 27, 2010 as DOI: 10.1124/jpet.110.176677
This article has not been copyedited and formatted. The final version may differ from this version.

$V_{plasma,TRZ}/F_{TRZ}$ represents a composite term combining both the triazolam volume of distribution and its oral bioavailability which were not resolved independently. The induction ratio, M, was used to account for the impact of enzyme induction on triazolam disposition following rifampicin pretreatment and is defined as follows:

$$M = \frac{CYP3A11}{CYP3A11_{(0)}} \quad (15)$$

where CYP3A11 represents the time-variable enzyme activity (as previously described in equation 11) and $CYP3A11_{(0)}$ is the basal enzyme activity. In naive or vehicle treated mice, where induction has not occurred, CYP3A11 enzyme activity would be equivalent to the basal activity and the ratio would collapse to unity.

Data from multiple animals were pooled and all PK-PD model fittings and parameter estimations were performed by nonlinear regression analysis using ADAPTII with the maximum likelihood method (Biomedical Simulations Resource, Los Angeles, CA). The variance models for rifampicin and triazolam pharmacokinetics (equation 16) and for the pharmacodynamics (equation 17) are given by:

$$\mathrm{Var}(\sigma, \theta, t_i) = (\sigma_1 + Y(\theta, t_i))^2 \quad (16)$$

$$\mathrm{Var}(\sigma, \theta, t_i) = {\sigma_2}^2 * Y(\theta, t_i)^{\sigma^2} \quad (17)$$

where Y represents the predicted value; σ_1 and σ_2 are the variance parameters which were fitted, and θ represents the structural parameters.

The goodness-of-fit was determined by visual inspection, Akaike Information Criterion, Schwartz Criterion, examination of the residuals and the coefficient of variation of the parameter estimates.

Results

***Cyp3a11* Induction in SXR Humanized Mouse Hepatocytes.** Following 3 days of treatment with rifampicin, RNA expression of *Cyp3a11* in the hepatocytes was increased in a concentration-dependent manner (Fig. 2). Non-linear regression analysis of the concentration-response curve yielded $SC_{50,RIF}$ and $S_{max,RIF}$ estimates of 6.2 μM and 7.86-fold, respectively (Table 3).

Rifampicin Pharmacokinetics. The 3-day time course of serum and liver rifampicin concentrations after 10 mg/kg oral administration (dosed once a day for 3 days) is shown in Fig. 3. The serum C_{max} for rifampicin following the 1st, 2nd and 3rd dose (days 1, 2 and 3) were 10.2, 16.7 and 10.0 μM, respectively and the corresponding liver C_{max} were relatively higher at 38.7, 44.1 and 26.0 μM, respectively. Similarly, total liver concentrations of rifampicin were greater than those observed in serum on all days of the study (average liver-to-serum AUC ratio = 4.3). The day 1, 2 and 3 serum $AUC_{0\text{-}24h}$ were 120, 254 and 206 μM*h whereas the corresponding liver AUC values were 571, 1036 and 866 μM*h. A modest increase in rifampicin exposure in the serum and liver on day 2 and 3 of dosing relative to day 1 is likely due to drug accumulation after repeat administration. Twenty-four hours following the last dose, the C_{max} and AUC on day 4 were 2.07 μM and 34.3 μM*h in the serum and 11.7 μM and 235 μM*h in the liver, respectively (Table 1). In order to describe the entire time-course of observed serum and liver rifampicin concentrations, a semi-PBPK model was developed. The model appears to provide a reasonable fit of the observed serum and liver rifampicin concentrations with reasonable variability in parameter estimation (Fig. 3 and Table 2).

Pharmacodynamics of *Cyp3a11* Induction *in vivo*. The *Cyp3a11* mRNA levels in vehicle treated animals remained relatively constant on days 1 and 4 (data not shown), indicating that baseline levels were stationary. After rifampicin administration, the *Cyp3a11* message began increasing between 8-24 h following the first dose (Fig. 4). *Cyp3a11* message levels reached a maximum by the end of day 2 which was sustained throughout days 3 and 4 and trending back toward baseline 48 h after the last dose of rifampicin. The CYP3A11 activity profile, as shown in Fig. 5, followed a similar increase as *Cyp3a11* mRNA with a comparable lag-time in the observed elevations relative to baseline. As expected, the baseline CYP3A11 enzyme activity was also stationary (data not shown). The observed stimulation of *Cyp3a11* mRNA production and subsequent elevations in CYP3A11 activity were adequately described using the *in vitro* derived estimates of $S_{max,RIF}$ and $SC_{50,RIF}$ which were fixed as constants in the model. The temporal profiles of *Cyp3a11* mRNA and CYP3A11 enzyme activity were captured well by this model (Fig. 4-5). The values of the estimated *Cyp3a11* dynamics are given in Table 3.

Triazolam Pharmacokinetics. As shown in Fig. 6, the serum pharmacokinetics of triazolam (4 mg/kg; P.O.) was assessed in mice 72 h after pretreatment with either 10 mg/kg rifampicin or vehicle (P.O.; once a day for 3 days). In vehicle treated mice, the serum concentrations were reasonably well described using a simple one-compartment model with first-order rates of absorption and elimination (Table 2 and Fig. 6). As described in Table 4, the predicted serum triazolam AUC in vehicle treated mice was close to the observed value; however, the predicted C_{max} was nearly two times lower than the observed value. In order to account for the impact of *Cyp3a11* induction on the

disposition of triazolam in the serum, its elimination rate was multiplied by a ratio of the time-variable enzyme activity over the basal enzyme activity (Equation 15). The previously determined triazolam pharmacokinetic parameters determined from fitting of the vehicle treated data (Table 2) were fixed and along with all the other final model parameters the concentration vs time profile of triazolam following 10 mg/kg rifampicin pretreatment was simulated. The C_{max} and AUC predictions from the final model are given in Table 4. The simulated triazolam pharmacokinetic profile agreed well with the observed data obtained from rifampicin pretreated mice.

Discussion

The pharmacokinetics of rifampicin in SXR humanized mice were comparable to previously published studies conducted in wild-type mice indicating that genetic modifications do not alter rifampicin pharmacokinetics (Bruzzese et al., 2000; Kim et al., 2008). Additionally, these data were comparable to previously reported data from our group in SXR humanized mice (Kim et al., 2008). The semi-physiologic pharmacokinetic model was used to describe rifampicin absorption from the gut into the liver and subsequent distribution into the central serum compartment. This approach provides a better representation of the physiological factors governing absorption, distribution and elimination than traditional mammillary models. While the present model does not take non-hepatic tissue distribution/elimination into consideration, it adequately described the observed liver and serum disposition of rifampicin. Moreover, with the hepatic elimination of rifampicin being described by a well-stirred model, known physiologic parameters (V_H, Q_H) and rifampicin mouse plasma protein binding ($f_{u,RIF}$) were able to be used as model constants. The final approximations of $CL_{H,RIF}$, $F_{H,RIF}$ and $V_{plasma,RIF}$ were consistent with what is known regarding rifampicin pharmacokinetics in mice being a low extraction compound with nearly complete gastric absorption (Bruzzese et al., 2000; Kim et al., 2008). A similar model was previously reported by Gordi et al to describe the pharmacokinetics of an anti-malarial drug, artemesin, in humans (Gordi et al., 2005) and allows hepatic rifampicin concentrations to be tied directly to its effects on hepatic enzymes (CYP3A11).

The data from this study illustrates that chronic oral administration of rifampicin results in elevations of *Cyp3a11* mRNA leading to a downstream increase in the

CYP3A11 enzyme activity and is consistent with prior observations in the literature (Xie et al., 2000; Gonzalez and Yu, 2006). To the best of our knowledge, this is the first study examining the entire time-course of PXR-mediated enzyme induction by rifampicin *in vivo*. As noted with other inducers, we observed a significant time delay between rifampicin administration and the onset of induction, with the peak response occurring approximately 48 h after the first dose of rifampicin (Gordi et al., 2005; Magnusson et al., 2006). This delayed onset is related to the complex series of events which must occur in order to trigger an increase in transcription (Moore et al., 2002; Milnes et al., 2008). We accounted for this temporal delay by using a series of transduction compartments which introduces time lags between the rifampicin liver concentration and the increase in mRNA levels. The final estimated 21 h delay for the initiation of induction is similar literature estimates for other CYP inducers in both human (Gordi et al., 2005) and rat (Magnusson et al., 2006). As mentioned previously, rifampicin liver concentrations served as the driving function for stimulation of mRNA production. Subsequently, the enhanced transcription of *Cyp3a11* mRNA regulates the increases in CYP3A11 enzymatic activity. The elevations in both the mRNA and enzyme activity were adequately captured by the model.

On day 4, animals dosed for three days with vehicle or rifampicin received triazolam orally to assess the impact of induction on the pharmacokinetics of a CYP3A11 probe substrate. There was a five-fold reduction in the triazolam serum AUC in rifampicin-treated mice was observed relative to the vehicle group (Table 4). These data are comparable to previous a study, although in that study the time-course of induction was not fully characterized (Kim et al., 2008). The pharmacokinetic model for triazolam

was constructed based on the concentration vs time relationship in the vehicle treatment group and it appears to adequately capture the observed data. To account for the impact of enhanced CYP3A11 activity on triazolam pharmacokinetics, we integrated a ratio of the time-variable CYP3A11 enzyme activity and basal enzyme activity. In vehicle treated mice, where no induction occurred, CYP3A11 activity equaled the basal activity and the ratio collapsed to unity. After rifampicin pretreatment, the time-variable CYP3A11 enzyme activity increased yielding reductions in triazolam exposure. Using this approach, the simulated triazolam pharmacokinetics in rifampicin-treated mice was consistent with the observed data. Our model provided a better prediction of the observed triazolam AUC; while the C_{max} was under-estimated which may be due to the limited amount of data collected during the triazolam absorption phase. The current SXR humanized mouse lacks the expression of gut PXR (mouse and human) due to the knock-out of mouse PXR and targeted expression of hPXR in the liver (via albumin promoter) (Xie et al., 2000). Therefore, rifampicin cannot induce gut *Cyp3a11* RNA, which might have reduced the absorption of triazolam by induction of gut-first pass metabolism. However, the ability to predict fold changes based upon AUC should be sufficient for assessment of potential DDI occurrences.

The attractive feature of this model is that it utilizes the *in vitro Cyp3a11* RNA induction potency estimates determined from humanized mouse hepatocytes as fixed model constants. It is conceivable that by integrating *in vivo* pharmacokinetic data and *in vitro* induction potency, one could predict the induction profile in mice for unknown compounds during the stages of drug discovery and approximate a potential fold induction in human. The main assumption of this approach is that the synthesis and

degradation rates of mRNA and enzyme are compound independent and the induction potential would be driven by the inducer potency and its hepatic concentrations. Based upon our fitted parameter estimates, the half-life for synthesis and degradation of CYP3A11 enzyme in mouse was 0.02 and 0.6 h, respectively. Values for human CYP3A4 degradation half-lives are reported to be within the range of 26 to 140 h (Yang et al., 2008) and are at least 40 times longer than our estimates for mouse CYP3A11. There are several potential explanations for this difference. There could be differences in the turnover rate of actual enzyme (i.e. human CYP3A4 vs mouse CYP3A11). Although, the reported turnover half-lives of a variety of human hepatic CYPs appear to be greater than 20 h (Ghanbari et al., 2006). Another explanation is that there may be species differences in the hepatic CYP turnover rates wherein mice have a quicker turnover than human. While plausible, Magnusson et al have reported enzyme turnover half-lives *in vivo* for a variety of rat CYPs in the range of ~40 h which are consistent with values reported for human (Magnusson et al., 2006). A more probable explanation for this discrepancy is likely related to the model predicted estimate of CYP3A11 degradation rate. In the present study, the pharmacodynamic effect of rifampicin was only monitored for four days after the initial dose of rifampicin. The levels of *Cyp3a11* mRNA and enzymatic activity had not returned to pre-dose baseline levels and therefore, the reliability of the estimate of the enzyme degradation rate could be suspect. While an extended sampling paradigm would be required to adequately capture the entire pharmacodynamic profile, the present model was able to anticipate the effect of induction on the CYP3A11 probe-substrate pharmacokinetics.

In a drug discovery setting, the proposed PK-PD model, combined with *in vitro* potency estimates from humanized mice and *in vivo* plasma and liver exposure data could aid in the assessment of an unknown compounds induction potential in the stages of lead optimization/characterization. Given the possibility that the rate constants governing the time course of induction of the CYP3A pathway are compound independent, one could use the proposed model to simulate the effect of induction on the pharmacokinetics of a probe substrate for unknown compounds. The only required model inputs would be the *in vitro Cyp3a11* RNA induction potency in hepatocytes and an understanding of the inducer's pharmacokinetics in mice. Assuming the unknown compound has linear pharmacokinetics and not solely metabolized by CYP3A enzyme (i.e. not a victim of auto-induction), only a single dose pharmacokinetic study in mice with sampling of plasma and liver concentrations would be required. This would alleviate the need for multiple dose *in vivo* induction studies dramatically minimizing the compound requirements and in-life resources that are typically constrained in the discovery setting. Knowledge of target *in vivo* exposures required for efficacy would aid in dose selection for the pharmacokinetic screen so that therapeutic concentrations could be achieved. Moreover, information obtained from these exercises could be used to aid in subsequent induction studies in larger nonclinical species (e.g. non-human primates) as well as placing it into context with anticipated efficacious human exposure to enable design of clinical DDI studies.

Overall, the results from this study suggest that the SXR humanized mouse and proposed PK-PD model could be valuable in predicting the outcome of CYP3A4 induction in patients while reducing the amount of data required for such predictions.

However, there are caveats in using this approach that have to be taken into consideration. First, the PK-PD model assumes that metabolism, pharmacokinetics and liver exposure are similar between mouse and human. If there is significant deviation from this underlying assumption, the predictive power of the model would be diminished. Secondly, the lack of gut PXR expression can lead to an under-prediction of human induction if the inducer or probe-substrate (victim drug) undergoes extensive first-pass metabolism. Thirdly, the current mouse model expresses mouse CAR, not human CAR**.** Due to the cross-talk between PXR and CAR in inducing CYP3A (and CYP2B) enzymes, it would be ideal if both nuclear hormone receptors were humanized for prediction of human drug-drug interactions.

Acknowledgments

The authors greatly appreciate the critical review of the manuscript by Drs. Kimberly Lentz and Kenneth Santone as well as acknowledge the significant contributions of Ms. Camellia Symonowicz and Bristol-Myers Squibb In Vivo Study Group for animal breeding and study support.

Authorship Contributions

Participated in research designs: Raybon, Zheng, Sinz and Kim

Conducted Experiments: Pray and Zoeckler

Contributed new reagents and analytical tools: Morgan

Performed Data Analysis: Raybon and Kim

Wrote and Contributed to the writing of the manuscript: Raybon, Sinz and Kim

Footnotes

These studies were funded by Bristol-Myers Squibb Co., USA.

References

Bauer B, Yang X, Hartz AM, Olson ER, Zhao R, Kalvass JC, Pollack GM and Miller DS (2006) In vivo activation of human pregnane X receptor tightens the blood-brain barrier to methadone through P-glycoprotein up-regulation. *Mol Pharmacol* **70**:1212-1219.

Bruzzese T, Rimaroli C, Bonabello A, Mozzi G, Ajay S and Cooverj ND (2000) Pharmacokinetics and tissue distribution of rifametane, a new 3-azinomethyl-rifamycin derivative, in several animal species. *Arzneimittelforschung* **50**:60-71.

Davies B and Morris T (1993) Physiological parameters in laboratory animals and humans. *Pharm Res* **10**:1093-1095.

Ghanbari F, Rowland-Yeo K, Bloomer JC, Clarke SE, Lennard MS, Tucker GT and Rostami-Hodjegan A (2006) A critical evaluation of the experimental design of studies of mechanism based enzyme inhibition, with implications for in vitro-in vivo extrapolation. *Curr Drug Metab* **7**:315-334.

Gonzalez FJ and Yu AM (2006) Cytochrome P450 and xenobiotic receptor humanized mice. *Annu Rev Pharmacol Toxicol* **46**:41-64.

Gordi T, Xie R, Huong NV, Huong DX, Karlsson MO and Ashton M (2005) A semiphysiological pharmacokinetic model for artemisinin in healthy subjects incorporating autoinduction of metabolism and saturable first-pass hepatic extraction. *Br J Clin Pharmacol* **59**:189-198.

Hariparsad N, Carr BA, Evers R and Chu X (2008) Comparison of immortalized Fa2N-4 cells and human hepatocytes as in vitro models for cytochrome P450 induction. *Drug Metabolism and Disposition* **36**:1046.

Hewitt NJ, de Kanter R and LeCluyse E (2007a) Induction of drug metabolizing enzymes: a survey of in vitro methodologies and interpretations used in the pharmaceutical industry--do they comply with FDA recommendations? *Chemico-biological interactions* **168**:51-65.

Hewitt NJ, Lechón MJG, Houston JB, Hallifax D, Brown HS, Maurel P, Kenna JG, Gustavsson L, Lohmann C and Skonberg C (2007b) Primary hepatocytes: current understanding of the regulation of metabolic enzymes and transporter proteins, and pharmaceutical practice for the use of hepatocytes in metabolism, enzyme induction, transporter, clearance, and hepatotoxicity studies. *Drug metabolism reviews* **39**:159-234.

Kim S, Pray D, Zheng M, Morgan DG, Pizzano JG, Zoeckler ME, Chimalakonda A and Sinz MW (2008) Quantitative relationship between rifampicin exposure and induction of Cyp3a11 in SXR humanized mice: extrapolation to human CYP3A4 induction potential. *Drug Metab Lett* **2**:169-175.

Lin JH (2006) CYP induction-mediated drug interactions: in vitro assessment and clinical implications. *Pharm Res* **23**:1089-1116.

Magnusson MO, Karlsson MO and Sandstrom R (2006) A mechanism-based integrated pharmacokinetic enzyme model describing the time course and magnitude of phenobarbital-mediated enzyme induction in the rat. *Pharm Res* **23**:521-532.

McGinnity DF, Zhang G, Kenny JR, Hamilton GA, Otmani S, Stams KR, Haney S, Brassil P, Stresser DM and Riley RJ (2009) Evaluation of multiple in vitro systems for assessment of CYP3A4 induction in drug discovery: human

hepatocytes, pregnane X receptor reporter gene, and Fa2N-4 and HepaRG cells. *Drug Metabolism and Disposition* **37**:1259.

Milnes MR, Garcia A, Grossman E, Grun F, Shiotsugu J, Tabb MM, Kawashima Y, Katsu Y, Watanabe H, Iguchi T and Blumberg B (2008) Activation of steroid and xenobiotic receptor (SXR, NR1I2) and its orthologs in laboratory, toxicologic, and genome model species. *Environ Health Perspect* **116**:880-885.

Moore LB, Maglich JM, McKee DD, Wisely B, Willson TM, Kliewer SA, Lambert MH and Moore JT (2002) Pregnane X receptor (PXR), constitutive androstane receptor (CAR), and benzoate X receptor (BXR) define three pharmacologically distinct classes of nuclear receptors. *Mol Endocrinol* **16**:977-986.

Ripp SL, Mills JB, Fahmi OA, Trevena KA, Liras JL, Maurer TS and de Morais SM (2006) Use of immortalized human hepatocytes to predict the magnitude of clinical drug-drug interactions caused by CYP3A4 induction. *Drug Metabolism and disposition* **34**:1742.

Sinz M, Kim S, Zhu Z, Chen T, Anthony M, Dickinson K and Rodrigues AD (2006) Evaluation of 170 xenobiotics as transactivators of human pregnane X receptor (hPXR) and correlation to known CYP3A4 drug interactions. *Curr Drug Metab* **7**:375-388.

Tucker GT, Houston JB and Huang SM (2001) Optimizing drug development: strategies to assess drug metabolism/transporter interaction potential—toward a consensus. *Pharmaceutical Research* **18**:1071-1080.

Wilkinson GR (1987) Clearance approaches in pharmacology. *Pharmacol Rev* **39**:1-47.

Xie W, Barwick JL, Downes M, Blumberg B, Simon CM, Nelson MC, Neuschwander-Tetri BA, Brunt EM, Guzelian PS and Evans RM (2000) Humanized xenobiotic response in mice expressing nuclear receptor SXR. *Nature* **406**:435-439.

Yang J, Liao M, Shou M, Jamei M, Yeo KR, Tucker GT and Rostami-Hodjegan A (2008) Cytochrome p450 turnover: regulation of synthesis and degradation, methods for determining rates, and implications for the prediction of drug interactions. *Curr Drug Metab* **9**:384-394.

Zhu Z, Kim S, Chen T, Lin JH, Bell A, Bryson J, Dubaquie Y, Yan N, Yanchunas J, Xie D, Stoffel R, Sinz M and Dickinson K (2004) Correlation of high-throughput pregnane X receptor (PXR) transactivation and binding assays. *J Biomol Screen* **9**:533-540.

Figure Legends

Figure 1. A semi-physiologically based PK-PD model describing the hepatic and systemic disposition of rifampicin and *Cyp3a11* RNA induction. $k_{a,RIF}$: absorption rate constant, $CL_{H,RIF}$: hepatic elimination, V_H: physiological liver volume, $V_{plasma,RIF}$: systemic volume of distribution, Q_H: hepatic plasma flow, $F_{H,RIF}$: hepatic bioavailability, $E_{H,RIF}$: hepatic extraction, $CL_{int,RIF}$: intrinsic clearance, $f_{u,RIF}$: plasma unbound fraction, $k_{s,RIF}$: plasma-to-liver transfer rate constant. The stimulatory effects of liver rifampicin exposures on *Cyp3a11* mRNA levels ($Cyp3a11_m$) were described using 3 transit compartments in-series involving both capacity ($S_{max,RIF}$) and sensitivity ($SC_{50,RIF}$) parameters determined *in vitro*. τ: transduction delay, $k_{syn,CYP3A11}$: synthesis rate of CYP3A11, $k_{deg,CYP3A11}$: degradation rate of CYP3A11. Triazolam disposition in the plasma was described using a one-compartment model. $k_{a,TRZ}$: absorption rate constant, $k_{el,TRZ}$: elimination rate constant, M: ratio of time-variable enzyme activity (CYP3A11) and basal enzyme activity ($CYP3A11_{(0)}$).

Figure 2. Concentration-response curve for the induction of *Cyp3a11* RNA expression in SXR humanized mouse hepatocytes.

Figure 3. Time course of rifampicin concentrations in liver (●) and serum (○) following 3 days of chronic rifampicin treatment (10 mg/kg P.O.; Q.D.). Solid lines represent model-predicted profiles after simultaneous fitting of all pharmacokinetic data. Data represent raw data obtained from 3 mice per time point.

Figure 4. Time course of SXR-induced stimulation of hepatic *Cyp3a11* mRNA levels following 3 days of chronic rifampicin treatment (10 mg/kg P.O.; Q.D.). Data represent

raw data obtained from 3 mice per time point (●). Solid lines represent model-predicted profiles.

Figure 5. Time course of SXR-induced stimulation of hepatic CYP3A11 enzymatic activity following 3 days of chronic rifampicin treatment (10 mg/kg; P.O.; Q.D.). Data represent raw data obtained from 3 mice per time point (●). Solid lines represent model-predicted profiles.

Figure 6. Time course of triazolam plasma concentrations (4 mg/kg; P.O.) on day 4 after 3-day pretreatment with either vehicle (●) or rifampicin (○; 10 mg/kg; P.O.; Q.D.). Solid lines represent model-predicted profiles after simultaneous fitting of all pharmacokinetic data. Data represent raw data obtained from 3 mice per time point.

JPET Fast Forward. Published on December 27, 2010 as DOI: 10.1124/jpet.110.176677
This article has not been copyedited and formatted. The final version may differ from this version.

Table 1. Noncompartmental analysis of rifampicin concentration versus time profiles in mice

Day	Matrix	T_{max} (h)	C_{max} (μM)	$AUC_{0\text{-}24h}$ (μM*h)
1	Serum	4	10.2	120
	Liver	4	38.7	571
2	Serum	4	16.7	254
	Liver	1	44.1	1036
3	Serum	4	10.0	206
	Liver	4	26.0	866
4	Serum	8	2.07	34.3
	Liver	8	11.7	235

**Data are expressed as mean values from 3 mice per time-point per day*

JPET Fast Forward. Published on December 27, 2010 as DOI: 10.1124/jpet.110.176677
This article has not been copyedited and formatted. The final version may differ from this version.

Table 2. Estimated pharmacokinetic parameters for rifampicin and triazolam

Parameters	Value	CV (%)
Rifampicin Pharmacokinetics		
$k_{a,RIF}$ (h^{-1})	0.69	18.3
$k_{s,RIF}$ (h^{-1})	26.4	14.6
$V_{plasma,RIF}$ (L/kg)	0.90	14.8
$CL_{int,RIF}$ (L/h/kg)	0.087	7.9
Q_H (L/h/kg)	5.40[a]	N.E.
V_H (L/kg)	0.065[a]	N.E.
$f_{u,RIF}$	0.12[a]	N.E.
$E_{H,RIF}$	0.0019[b]	N.E.
$F_{H,RIF}$	1.00[b]	N.E.
$CL_{H,RIF}$ (L/h/kg)	0.010[b]	N.E.
Triazolam Pharmacokinetics (post-vehicle administration)		
$k_{a,TRZ}$ (h^{-1})	0.43	11.2
$k_{el,TRZ}$ (h^{-1})	27.9	114
$V_{plasma,TRZ}/F_{TRZ}$ (L/kg)	0.38	114

N.E. - Not Estimated.
[a]*Parameter fixed to literature/experimental value.*
[b]*Secondary parameter.*

JPET Fast Forward. Published on December 27, 2010 as DOI: 10.1124/jpet.110.176677
This article has not been copyedited and formatted. The final version may differ from this version.

Table 3. Estimated pharmacodynamic parameters

Parameters	Value	CV (%)
Pharmacodynamics		
τ (h)	7.94	10.1
γ	0.60	9.66
$k_{syn,CYP3A11}$ (h^{-1})	35.4	228
$K_{deg,CYP3A11}$ (h^{-1})	1.15[a]	N.E.
$S_{max,RIF}$ (fold)	7.86[b]	N.E.
$SC_{50,RIF}$ (μM)	6.2[b]	N.E.
Cyp3a11$_{m,(0)}$ (fold)	0.88	11.5
$CYP3A11_{(0)}$ (nM/h/mg)	28.5	5.59

N.E. - Not Estimated.
[a]*Secondary parameter.*
[b]*Parameter fixed to experimental value.*

JPET Fast Forward. Published on December 27, 2010 as DOI: 10.1124/jpet.110.176677
This article has not been copyedited and formatted. The final version may differ from this version.

Table 4. Observed vs predicted pharmacokinetics of triazolam in vehicle and rifampicin-treated mice

Treatment	C_{max} (nM)		$AUC_{0\text{-}8h}$ (nM*h)	
	Observed	Predicted	Observed	Predicted
Vehicle	853	442	882	1008
Treated	106	146	210	336
Fold Change	8	3	4	3

**Data are expressed as mean values from 3 mice per time-point.*

Figure 1

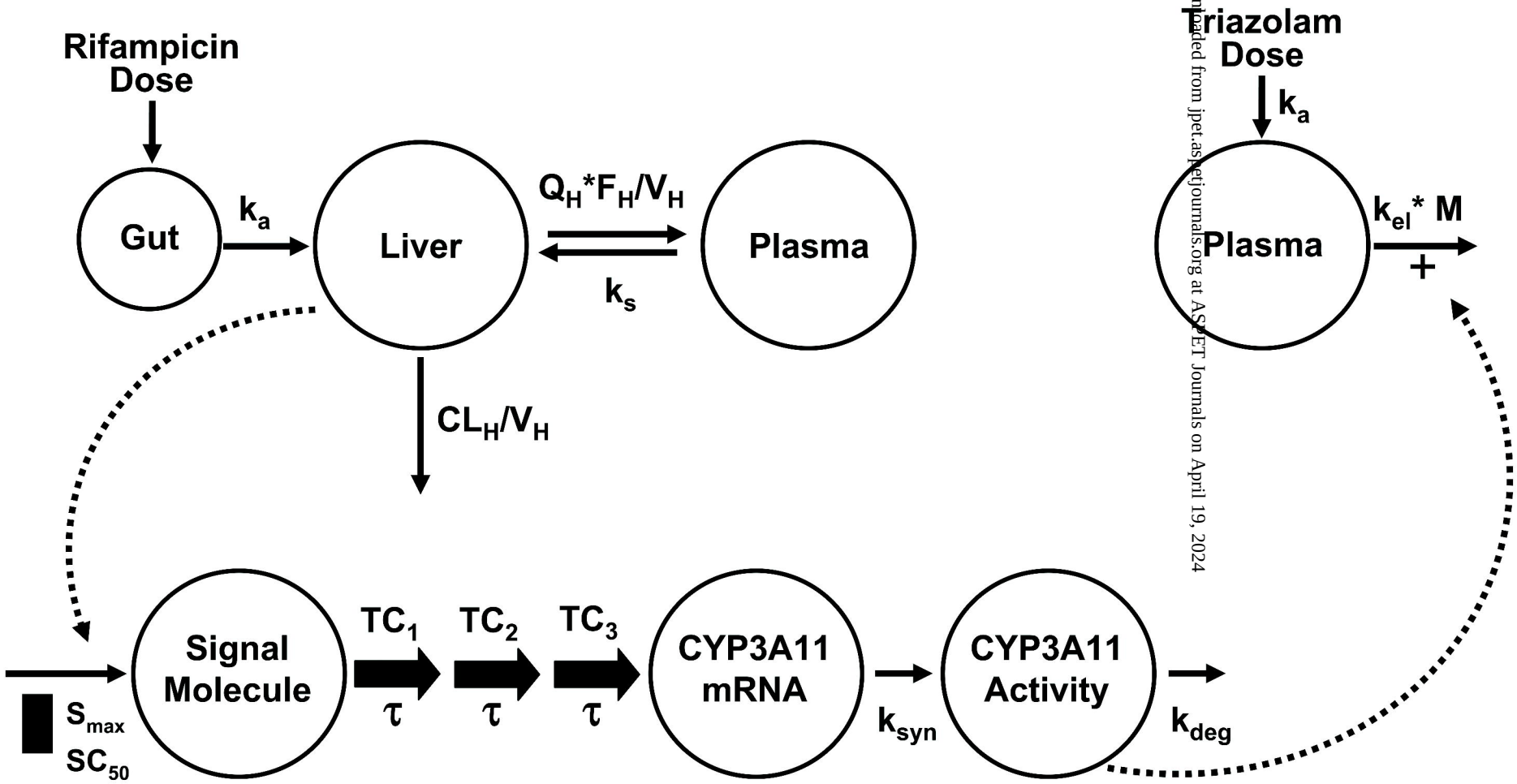

Figure 2

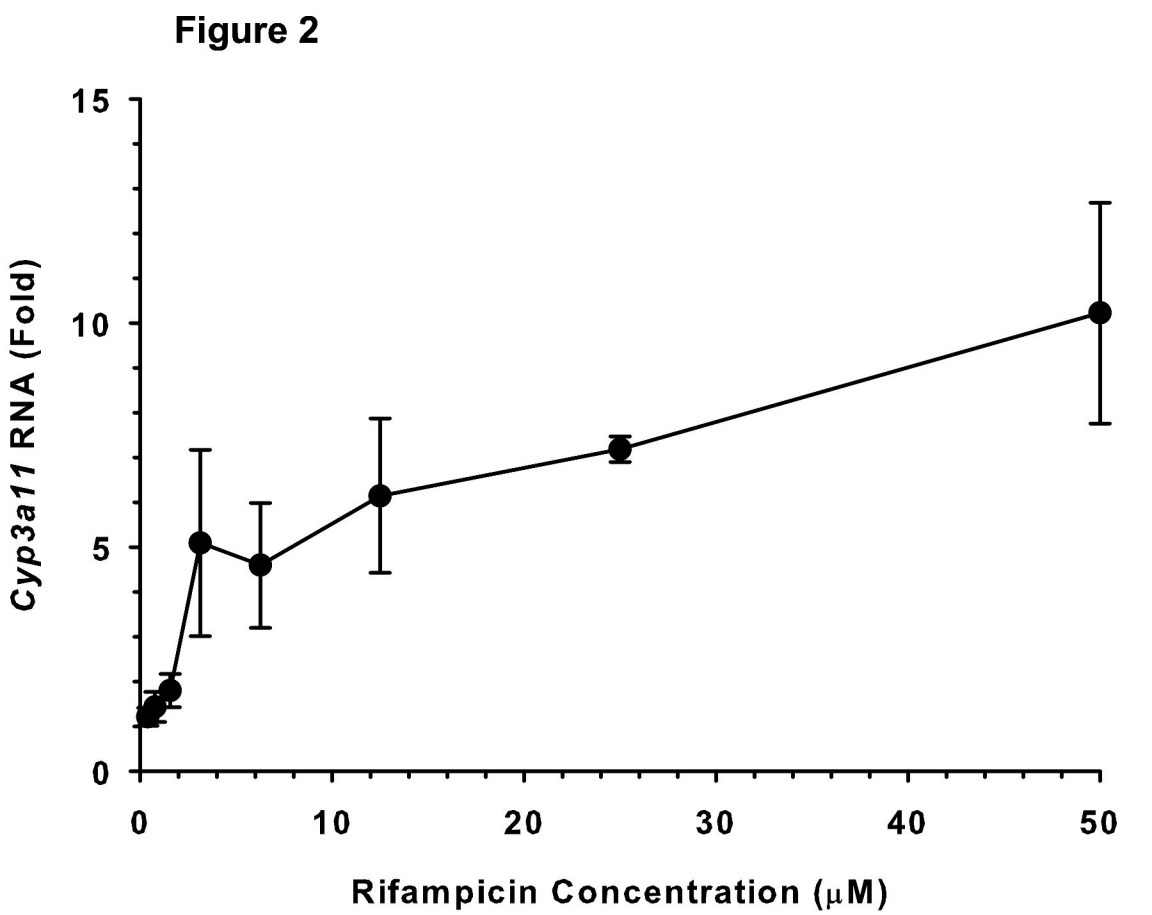
15
10
5
0
Cyp3a11 RNA (Fold)
0
10
20
30
40
50
Rifampicin Concentration (μM)

Figure 3

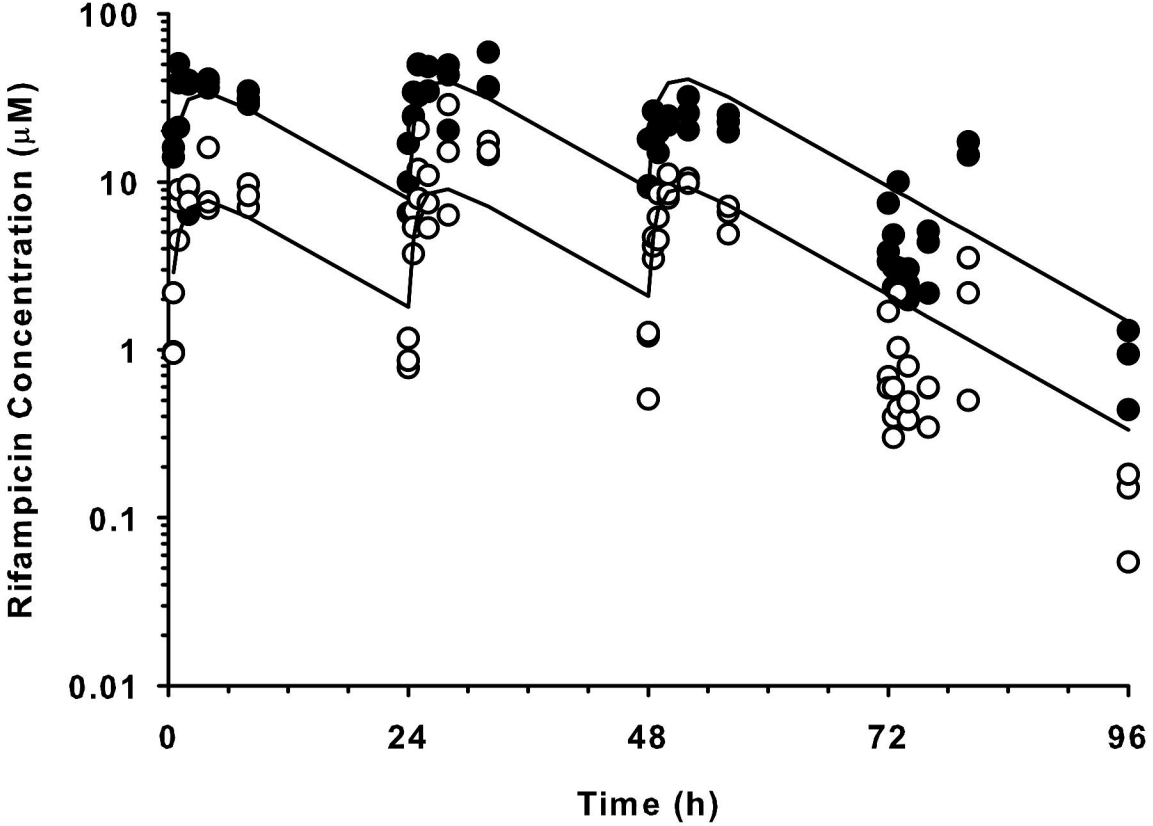
100
10
1
0.1
0.01
Rifampicin Concentration (μM)
0
24
48
72
96
Time (h)

Figure 4

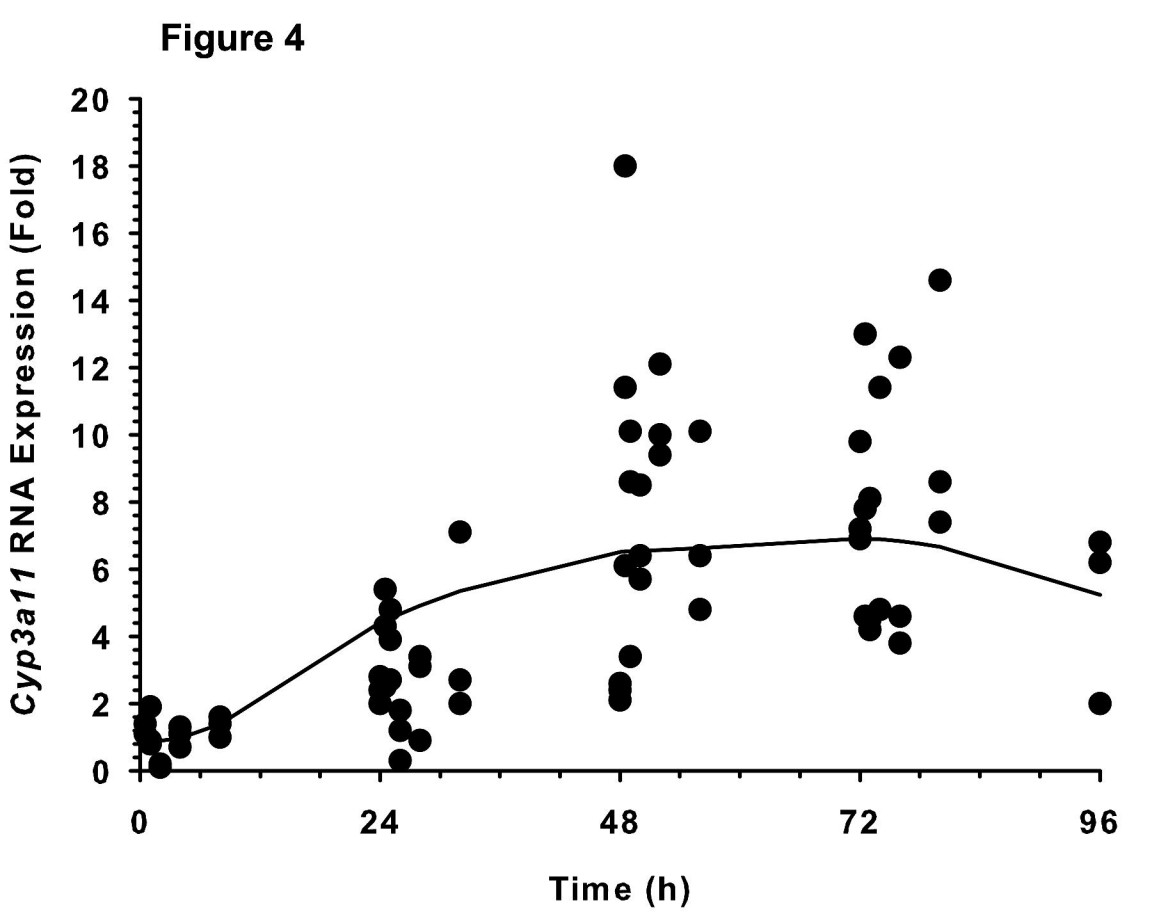
20
18
16
14
12
10
8
6
4
2
0
Cyp3a11 RNA Expression (Fold)
0
24
48
72
96
Time (h)

Figure 5

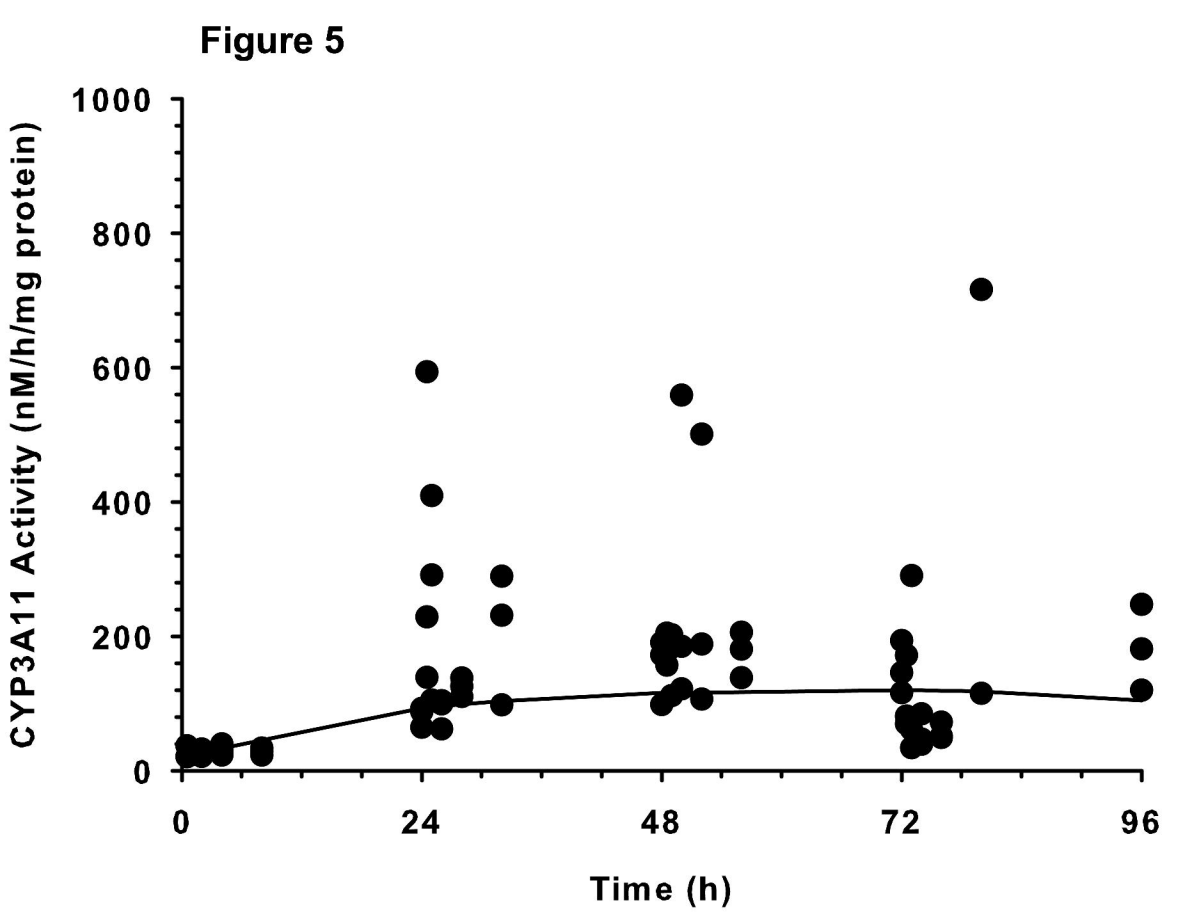
1000
800
600
400
200
0
CYP3A11 Activity (nM/h/mg protein)
0
24
48
72
96
Time (h)

Figure 6

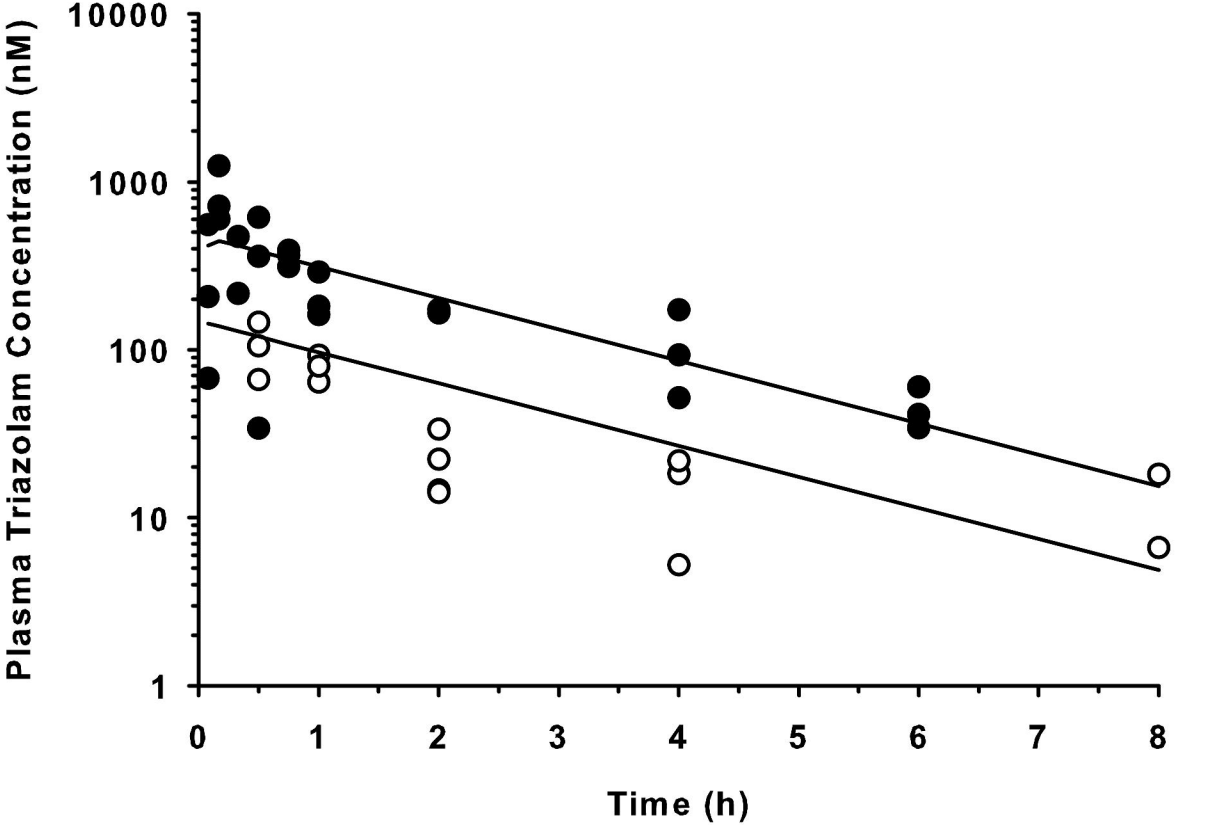
Plasma Triazolam Concentration (nM)
10000
1000
100
10
1
0
1
2
3
4
5
6
7
8
Time (h)